ARTICLE

Design of Surfaces for Liquid Crystal-Based Bioanalytical Assays

Aaron M. Lowe,[†] Byram H. Ozer,[‡] Yiqun Bai,[†] Paul J. Bertics,[‡] and Nicholas L. Abbott*[,†]

Department of Chemical and Biological Engineering and Department of Biomolecular Chemistry, University of Wisconsin, Madison, Wisconsin 53706

ABSTRACT Surface-induced ordering of liquid crystals (LCs) offers the basis of a label-free analytical technique for the detection of surface-bound biomolecules. The orientation-dependent energy of interaction of a LC with a surface (anchoring energy of LC), in particular, is both sensitive to the presence of surface-bound molecules and easily quantified. Herein, we report a study that analyzes a simple model of twisted nematic LC systems and thereby identifies surfaces with LC anchoring energies in the range of 0.5 μJ/m^2 to 2.0 μJ/m^2 to be optimal for use with LC-based analytical methods. Guided by these predictions, we demonstrate that analytic surfaces possessing anchoring energies within this range can be fabricated with a high level of precision (< 0.1 μJ/m^2) through formation of monolayers of organothiols (with ω-functional groups corresponding to oligoethyleneglycols and amines) on gold films deposited by physical vapor deposition at oblique angles of incidence. Finally, by using the human epidermal growth factor receptor (EGFR) as a model protein analyte, we have characterized the influence of the anchoring energies of the surfaces on the response of the LC to the presence of surface-bound EGFR. These results, when combined with ^{32}P-radiolabeling of the EGFR to independently quantify the surface concentration of EGFR, permit identification of surfaces that allow use of LCs to report surface densities of EGFR of 30−40 pg/mm^2. Overall, the results reported in this paper guide the design of surfaces for use in LC-based analytical systems.

KEYWORDS: liquid crystals • patterned surface chemistry • bioanalytical methods • chemically functionalized surfaces • imaging • affinity microcontact printed proteins • anchoring energies

INTRODUCTION

The development of analytical techniques for the detection of biomolecules such as DNA (1) and protein (2) molecules has been the subject of numerous prior studies (3−8). Array-based methods, in particular, hold potential for both basic research and clinical diagnostics because the sample volumes required are minimal (∼1 nL) and detection of multiple target molecules can be performed in parallel (9−11). A common detection scheme involves capture of the target molecule with a surface-immobilized antibody (the capture antibody), followed by sequential incubation with a primary antibody to the target molecule and then with a labeled (e.g., fluorescent or radioactive) secondary antibody directed towards the primary antibody (12, 13). Each antibody incubation increases the overall cost and complexity of the analytical scheme, particularly if multiple target molecules are to be detected simultaneously. To address this limitation, analytical techniques that do not require the use of primary and labeled secondary antibodies have been developed, including surface plasmon resonance (SPR) (14), mass spectrometry (MS) (15), and atomic force microscopy (AFM) (16). Although these techniques are sensitive, they each require use of complex instrumentation.

In this paper, we report an investigation that seeks to advance the use of liquid crystals (LCs) for the detection of biomolecules in surface-based assays. LC-based analytical techniques offer the potential for a relatively simple methodology that allows multiplexed and label-free detection of biomolecules without the need for secondary antibodies or complex instrumentation. Previously, we have reported the feasibility of LC-based methods to quantify the loadings of peptides and proteins presented at surfaces (17, 18) by measuring changes in the interaction energy of the LC with the biomolecule-decorated surfaces (the so-called anchoring energy). The approach involves the capture of polarized light images from a standard optical microscope and the use of an automated image analysis routine (19). By measuring changes in the anchoring energy of the LC on an analytic surface, past studies have demonstrated that LCs can be used to detect ∼1 ng/cm^2 of peptide or antibody on the analytic surface.

The anchoring energies of LCs at surfaces have been widely studied in the past in the context of LC-based display devices, where stable, precisely aligned LC phases are desired. Because display devices rely upon the application of an electric field so as to drive reordering of the bulk LC (Figure 1A), the anchoring energies of surfaces used in these devices are typically high (∼300 μJ/m^2) (20). In contrast, when surface-induced ordering of LCs is used to report the presence of surface adsorbates, surfaces with low anchoring energies are required. In this context (Figure 1B) (17−19, 21, 22), the collective ordering of the molecules (mesogens) within LC phases in contact with surfaces with low anchoring energies can be exploited as a form of

* Corresponding author. Phone: (608) 265-5278. Fax: (608) 262-5434. E-mail: abbott@engr.wisc.edu.
Received for review November 2, 2009 and accepted February 2, 2010
† Department of Chemical and Biological Engineering, University of Wisconsin.
‡ Department of Biomolecular Chemistry, University of Wisconsin.
DOI: 10.1021/am900753v

Published on Web 02/26/2010

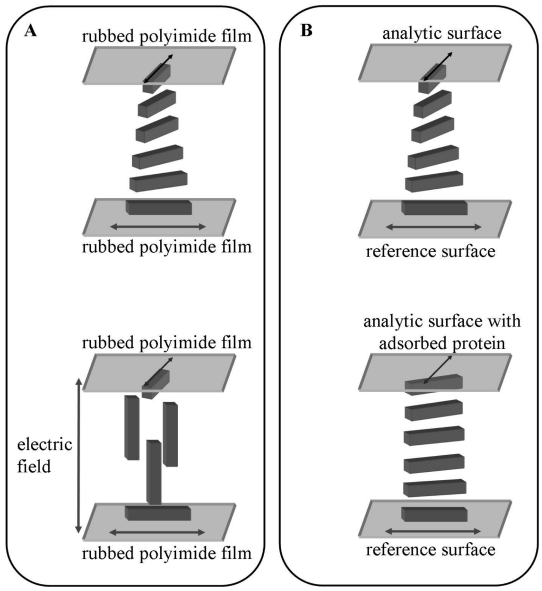

FIGURE 1. Schematic illustrations of (A) electric-field induced and (B) surface-induced ordering transitions in nematic LCs. In A, a twist distortion is induced in the LC by two polyimide films that have been mechanically rubbed in orthogonal directions (represented by the double ended arrows, top panel). Upon application of an electric field (bottom panel), the LC reorients out of the plane of the polyimide surfaces. In B, the LC is twisted by two surfaces with easy axes (represented by the double ended arrows, top panel) that have been defined by oblique deposition of gold films from a vapor and subsequent functionalization with self-assembled monolayers of organothiols. The twist angle of the LC is decreased in the presence of proteins bound to the analytic surface (bottom panel).

amplification; events at the molecular level (nanometers) occurring on the surface can be amplified into changes in the ordering of LC phases at the optical scale (micrometers). Because the majority of past studies of LC surface anchoring have been pursued in the context of display device applications, there have been comparatively few studies of low anchoring energy surfaces (23–26).

In particular, to date there have been no prior studies that have sought to design and fabricate surfaces with anchoring energies that are optimal for the detection of biomolecules using LCs (17–19). The study reported herein advances our understanding of LC-based analytical techniques by using a simple model to identify optimal anchoring energies that maximize the response of LCs to the presence of proteins captured on surfaces. We also demonstrate experimental approaches that allow the realization of surfaces that anchor LCs with energies that lie in the range identified to be optimal. Lastly, we report on the response of an LC to a protein analyte that is presented at surfaces engineered to possess the optimal anchoring energies. Specifically, we characterize the response of an LC to the presence of the epidermal growth factor receptor (EGFR), a 170 kDa transmembrane glycoprotein receptor (tyrosine kinase) that we selected because it represents a biologically relevant target. EGFR has been the subject of numerous studies because its over expression and/or mutation has been associated with a variety malignancies including carcinoma of the lung, head and neck (27, 28).

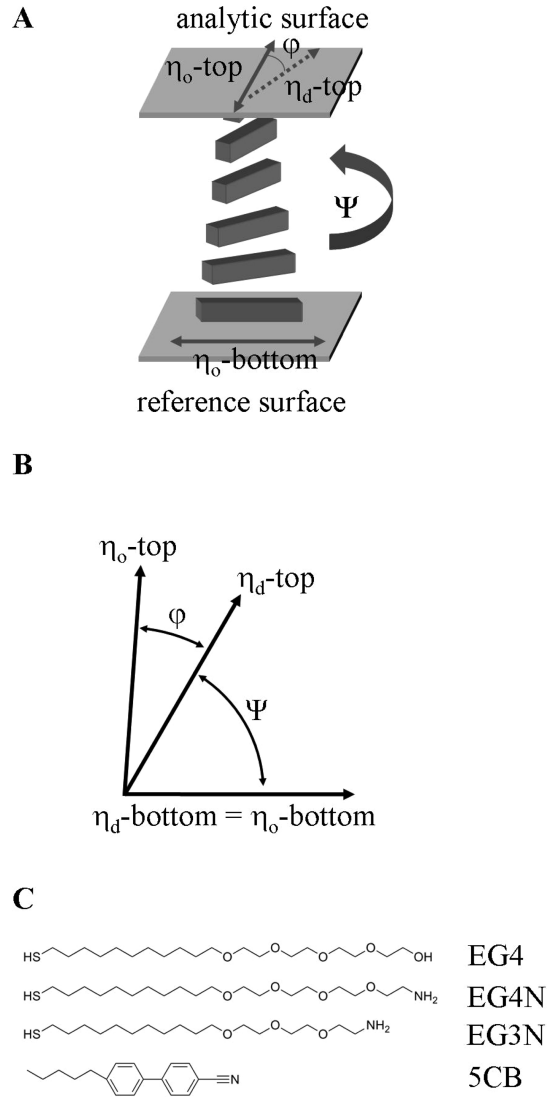

FIGURE 2. (A, B) Geometry of the twisted nematic LC cells in this study. The LC is aligned by easy axes on the reference surface (ηo-bottom) and analytic surface (ηotop) such that a twist of angle Ψ is introduced. The LC director near the analytic surface (η_d-top) deviates by an angle (φ) from the easy axis because of the strain (twist) of the LC, and the finite anchoring energy of the analytic surface. (C) Structure of the molecules used in this study.

The experimental approach used in the study reported in this paper relies on LCs that possess a twist distortion. Past studies have shown that changes in the anchoring energy of a nematic LC on a surface can be measured by using a twisted nematic liquid crystal (TNLC) optical cell (Figure 2A, B) (29). A TNLC is formed by confining a nematic LC between two surfaces that orient the LC mesogens in mutually orthogonal in-plane directions. The preferred direction of in-plane alignment of the LC is referred to as the easy axis, η_o. Control of the orientation of the easy axis of a surface can be achieved by using surface fabrication methods such as mechanical rubbing of polyimide films (30, 31), oblique deposition of metal (32) or oxide (33) films from vapor, self-assembly of carbon nanotubes on glass surfaces (34), and chemical functionalization of obliquely deposited gold films (22, 35, 36). Because the LC has a twist elastic modulus that opposes the twist distortion induced by the

confining surfaces, the resulting angle of twist exhibited by the LC, Ψ, is determined by the competition between the elastic energy stored in the bulk LC and the anchoring energy of the aligning surfaces. This competition causes the orientation of the LC near the surface to deviate from the easy axis (by an angle defined as φ). In our studies, we paired two surfaces, an analytic surface with anchoring energy W_{az} and a reference surface with sufficiently high anchoring energy that there was negligible deviation of the LC orientation from the easy axis of the reference surface. For optical cells with a known LC film thickness (d) and twist elastic constant (K_{22}), the anchoring energy of the analytic surface can be calculated using the so-called torque-balance model (29) as

$$W_{az} = \frac{2K_{22}\Psi}{d\sin(2\varphi)} \quad (1)$$

Because the sum of Ψ and φ must equal the angle between the easy axes of the analytic surface and reference surface (see Figure 2B), the anchoring energy W_{az} is a nonlinear function of Ψ. In this study, we analyzed the predictions of the torque-balance model (eq 1) to identify an optimal range of anchoring energies and LC film thicknesses that we predicted would lead to large changes in the LC twist angle induced by surface-bound adsorbates (EGFR in this study).

MATERIALS AND METHODS

Materials. All materials were used as received, unless otherwise noted. Fisher's Finest glass slides were obtained from Fisher Scientific (Pittsburgh, PA). Gold (99.999% purity) was obtained from International Advanced Materials (Spring Valley, NY). Titanium (99.99% purity) was obtained from PureTech (Brewster, NY). Polished silicon wafers were purchased from Silicon Sense (Nashua, NH). Tetraethylene glycol-terminated thiol (Figure 2C, $HS(CH_2)_{11}EG4$, referred to as EG4), EG4N (Figure 2C, $HS(CH_2)_{11}EG4NH_2$*HCl), and EG3N (Figure 2C, $HS(CH_2)_{11}EG3NH_2$*HCl) were obtained from Prochimia (Gdansk, Poland). Pentadecanethiol, hexadecanethiol, 2-aminoethanethiol hydrochloride (AET), and *N*-hydroxysuccinimide (NHS) were obtained from Sigma-Aldrich (Milwaukee, WI). 1-Ethyl-3-(3-dimethylaminopropyl)carbodiimide hydrochloride (EDC) was obtained from Pierce Biotechnology (Rockford, IL). Liquid crystal 4′-pentyl-4-cyanobiphenyl (5CB, Figure 2C) was obtained from EM Industries (New York, NY), and sold under the trademark name Licrystal (K15). Anhydrous ethanol containing 5% isopropyl alcohol and 5% methyl alcohol as denaturants was obtained from Sigma-Aldrich and purged with argon gas for 1 h prior to use. Poly(dimethylsiloxane) (PDMS) elastomeric stamps were prepared using Sylgard 184 silicone elastomer kit obtained from Dow Corning (Midland, MI). IgG-free BSA was purchased from Jackson Immunoresearch (West Grove, PA). Radioactive [γ-^{32}P] ATP was purchased from Amersham/GE Health Care. Monoclonal murine anti-EGF receptor IgG clone H11was obtained from LabVision (Fremont, CA). Monoclonal murine IgG isotype control antibodies were purchased from eBioscience (San Diego, CA). All antibodies were obtained at 1 mg/mL concentration and free of BSA and azide and were used as is or following dilution with phosphate buffered saline (PBS: 138 mM NaCl, 8 mM Na_2HPO_4, 2.8 mM KCl, 1.5 mM KH_2PO_4, Sigma-Aldrich, Milwaukee, WI), pH 7.4.

Preparation of Gold Substrates. Glass slides, cleaned as described previously (18, 22), were positioned within the chamber of an electron beam evaporator such that the incident angle of metal flux onto the substrate could be controlled. The incident angles (θ_i, with respect to the surface normal) were measured with a digital level, with an accuracy of ±0.5°. All metal films were deposited at chamber pressures $<2 \times 10^{-6}$ Torr at deposition rates of 0.2 Å/s. A thin film of titanium (thickness of 42−60 Å) was deposited onto the glass substrate to serve as an adhesion layer between the glass and semitransparent film of gold (thickness of 105−140 Å). All gold substrates were used within 1 h of removal from the evaporator chamber.

Formation of Patterned Self-Assembled Monolayers (SAMs). A PDMS elastomeric stamp was cast against a silicon wafer that was silanized with (tridecafluoro-1,1,2,2,-tetrahydrooctyl)-1-trichlorosilane vapor (18 hours under vacuum) to aid in the release of the PDMS. After curing the PDMS for at least 18 h at 65 °C, the stamp was peeled from the wafer and ultrasonicated in a solution of 2:1 ethanol/water for 10 min × 3 cycles. The PDMS was then cut into small strips (5 × 1 mm) that were inked with a 2 mM ethanolic solution of hexadecanethiol for 30 s followed by drying with a stream of nitrogen gas. The PDMS stamps were placed into conformal contact with an obliquely deposited gold slide for 5 min and peeled away. The slide surface was rinsed with ethanol, and the non-functionalized gold surface was incubated in an ethanolic solution of an organothiol for 18 hours unless noted otherwise. The hydrophobic SAM formed from contact printing of hexadecanethiol served to confine the thiol solution to the bare regions of the gold film, and also to align the LC in a direction that is parallel to the in-plane direction of gold deposition (18, 22). After thiol incubation, the slides were rinsed sequentially with copious amounts of ethanol, water, and ethanol, and then dried under a stream of gaseous nitrogen. Because a number of past studies have concluded that SAMs formed from organothiols can oxidize upon storage (37−39), we used all of the gold films in this study immediately after chemical functionalization in order to minimize any possible influence of oxidation on our results.

Affinity Microcontact Printing of EGFR. The capture, transfer, and subsequent quantification of EGFR were performed as previsouly described (40, 41). These procedures are also described in detail in the Supporting Information.

Fabrication of Optical Cells. Optical cells were fabricated by pairing an analytical surface with a reference surface such that the gold films were mutually oriented as depicted in Figure 2A. The reference surface was a gold film (deposited at an angle of 64° relative to the surface normal) that was functionalized with pentadecanethiol by immersion into a 1 mM ethanolic solution for 18 h. This type of surface strongly anchors the LC. The angle between the in-plane direction of gold deposition on the reference surface and analytic surface was nominally 80°. The analytic surface and reference surface were spaced apart using combinations of Mylar spacers that allowed us to form cavities between the two surfaces that ranged from 5−50 μm. The cavity between the two surfaces was filled with 5CB that was heated into its isotropic phase (∼50 °C). Optical measurements of the LC cell were carried out after cooling the cell to 26 °C for 30 min.

Measurement of the Twist Angle of the Liquid Crystal. We measured the twist angle of the LC by our previously reported automated analysis method (19). The optical cell containing the LC was placed between crossed polarizers with the input polarizer facing the reference surface. The easy axis of the LC on the reference surface was aligned parallel to the input polarizer using the technique described by Lien (42). Briefly, an iterative process was used to minimize the transmission of 546.5 nm light through the regions functionalized with hexadecanethiol on the analytic surface. This was accomplished by alternately rotating the sample between the stationary polarizers, followed by rotation of the analyzer. The transmission of light was minimized at each of the iterations. Three iterations were typically sufficient. Images were obtained using a polarized

light microscope (BX60, Olympus) equipped with an X−Y translation stage and a digital camera (2.8 f-stop, 1/800 s shutter speed, 1024 × 768 resolution). Consistent settings of the light intensity were used (aperture set at one-half maximum, and lamp intensity set at four-tenths maximum) for individual samples. The lamp intensity was set at four-tenths of maximum to ensure that the images did not saturate during rotation of the analyzer. The analyzer was rotated at 10° increments, with images obtained at each analyzer position. The fraction of light transmitted through the optical cell, T_{wg}, was fit to the function

$$T_{wg} = \cos^2(\Psi - \gamma) \quad (2)$$

where Ψ is the twist angle of the LC (Figure 2A, B) and γ is the position of the analyzer relative to the input polarizer (γ = 0−170°). The fit was performed at each pixel of the family of polarized images of each optical cell using an algorithm implemented in MATLAB (version 7.3.0, 2006b) to yield a two-dimensional matrix with elements representing the values of the twist angle at each pixel.

RESULTS AND DISCUSSION

Determination of Optimal Anchoring Energies. The first goal of our study was to identify the optimal range of anchoring energies and LC film thicknesses such that changes in the azimuthal anchoring energy caused by binding of biomolecules would result in measurable changes in LC orientation (i.e., changes in LC twist angle). We directed our focus to twist angle measurements because the twist angle of nematic LCs can be easily measured using optical microscopy-based techniques in a spatially resolved manner (19). The twist angle can then be used to calculate the anchoring energy and correlated to the loading of protein molecules bound to the surface (17). By using optical microscopy techniques and surfaces with uniform anchoring energies, we note that we typically measure a standard deviation in twist angles (sample-to-sample and within a single sample) that ranges from 0.1−1.0°. This level of precision is a consequence, in part, of optical effects such as lens flair and light scattering.

Inspection of eq 1 reveals that the twist angle of a TNLC (defined as Ψ) is governed by the twist elastic constant (K_{22}, which is a property of the LC), the angle of departure of the LC director from the easy axis (φ), the LC film thickness (d) and the anchoring energy W_{az}. For the purposes of the study reported in this paper, we have constrained K_{22} to correspond to a nematic phase of 4′-pentyl-4-cyanobiphenyl at room temperature (5CB, K_{22} = 3.81 pN) (43), and we have set $\Psi + \varphi$ to a value of 80°. We focus our attention on the influence of W_{az} and d on the twist angle of the LC. We limit the values of d to lie between 4 and 50 μm, which corresponds to the range of experimentally accessible LC film thicknesses.

Figure 3A shows the twist angle (Ψ) of nematic 5CB calculated as a function of the LC film thickness (4−50 μm) and LC anchoring energy (0−10 μJ/m^2). Inspection of Figure 3A reveals that the twist angle of the LC is insensitive to changes in the value of the LC anchoring energy that are greater than ~0.5 μJ/m^2 for thick LC films (d = 50 μm) and 2 μJ/m^2 for thin LC films (d = 4 μm). This point is detailed in

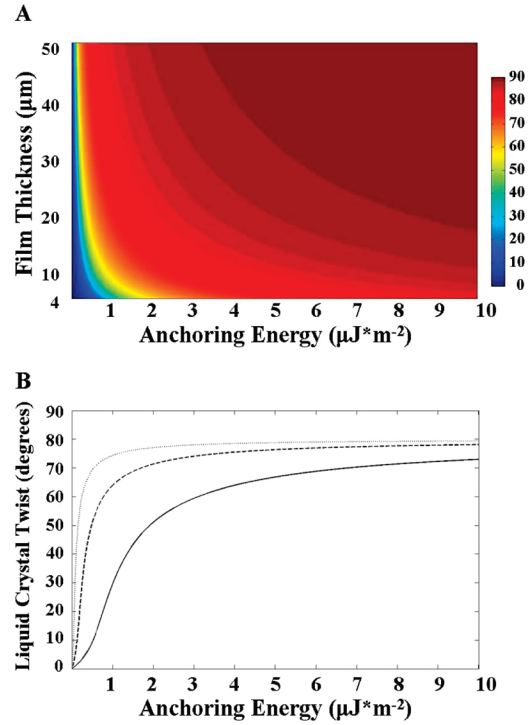

FIGURE 3. Twist angles of LCs calculated from the torque-balance equation. Calculations are for 5CB and assume that the easy axes of the confining surfaces are oriented 80° relative to one another. (A) Landscape of LC twist angles illustrating that the greatest change in twist angle as a function of anchoring energy occurs at low values of the anchoring energy and film thickness. (B) Plots of LC twist versus azimuthal anchoring energy for LC films thicknesses of 50 μm (dotted line), 16 μEm (solid line).

Figure 3B, where the twist angle of the LC is plotted as a function of the anchoring energy for three LC film thicknesses. The LC twist angle is insensitive to changes in the anchoring energy at high values of anchoring energy because the torque generated by the twist of the LC is insufficient to perturb the orientation of the LC at the confining surfaces away from the easy axis. Although a decrease in LC film thickness can be used to increase the magnitude of the torque generated by the LC, a decrease in LC film thickness from 50 μm to 4 μm increases the upper bound on the anchoring energy to only ~2−3 μJ/m^2. In summary, the key conclusion that emerges from this simple analyses of eq 1 is that optimal anchoring energies for surfaces to be used in LC-based bioanalytical methods will lie in the range of 2 to 0.5 μJ/m^2. If surfaces with anchoring energies of LCs that are substantially larger than these values are used, the uncertainty in experimental measurements of the LC twist angle will lead to large errors on the calculated anchoring energies. For example, if a surface with a LC anchoring energy of 5 μJ/m^2 is used in combination with a LC film thickness of 50 μm, an uncertainty in measurement of the LC twist angle of ±0.5° would lead to an uncertainty in the anchoring energy of approximately ±2 μJ/m^2. Below we describe the results of a study that sought to engineer surfaces with anchoring energies in the range of 2.0−0.5 μJ/m^2.

Tuning Anchoring Energies of LCs through Manipulation of the Angle of Deposition of Gold Films. The approach we used to tune the anchoring ener-

gies of surfaces was based on gold films deposited from a vapor at an oblique angle of incidence. Past studies have demonstrated that when metal films are deposited onto glass substrates by vapor deposition at an oblique angle of incidence, the angle of incidence between the deposition source and glass substrate has a substantial influence on the final film structure (44) and anchoring energy (32). In these studies, x-ray diffraction (XRD) measurements were combined with optical second-harmonic generation spectroscopy (SHG) to show that the polycrystalline gold grains of the obliquely deposited film are terminated mainly with (111) facet planes and that an in-plane texturing exists in the terminating facet planes such that one of the [110] axes in the facet is oriented perpendicular to the plane of incidence of the gold during deposition. Atomic force microscopy (AFM) measurements have also demonstrated that oblique vapor deposition of gold films leads to anisotropic surface topography (statistical corrugation) on spatial scales comparable to the sizes of individual gold grains (~30 nm) (32). It is well known that corrugated surfaces can orient LC phases (45). Finally, it has also been shown that the chemical composition of SAMs formed on these obliquely deposited metal films can alter the anchoring energy of LCs on the surfaces (22). To date, however, there has been no systematic study that demonstrates control of the anchoring energy over the range identified above to be optimal for bioanalytical detection. Because of the broad relevance of ethylene glycol-terminated monolayers for bioanalytical systems, we report below measurements of the anchoring energies of LCs on SAMs formed from tetra(ethylene glycol)-terminated alkanethiols (EG4, Figure 2C) and amino-tetra(ethylene glycol)-terminated alkanethiols (EG4N, Figure 2C) as a function of the angle of deposition of the gold used to prepare the gold films. SAMs formed from EG4 have been shown to inhibit non-specific adsorption of protein molecules from solution (46–48), while the amine functionality of SAMs formed from EG4N can be used to immobilize biomolecules through standard bioconjugate chemistry (17, 21), capture proteins during affinity contact printing (49–52) or promote cell adhesion (mediated by adsorbed proteins) (53, 54). We sought to determine how the terminal functional groups of these SAMs would influence anchoring energies when the SAMs were formed on gold films deposited at various angles of incidence.

Figure 4 shows the anchoring energies of SAMs formed from EG4 supported on gold films deposited at angles ranging from 15–40° relative to the surface normal. All anchoring energies presented are averages based on a minimum of three samples, with error bars that represent 95% confidence intervals. Inspection of Figure 4 shows that the anchoring energies increase monotonically with the deposition angle, with a minimum value of 0.45 ± 0.09 μJ/m^2 measured at 15° and a maximum value of 2.75 ± 0.58 μJ/m^2 measured at 40°. By applying a linear fit to the data set (a slope of 0.09 μJ/m^2/°), we extrapolate the data to predict that a gold deposition angle of 49° would lead to an anchoring energy of 3.40 μJ/m^2, a prediction that agrees

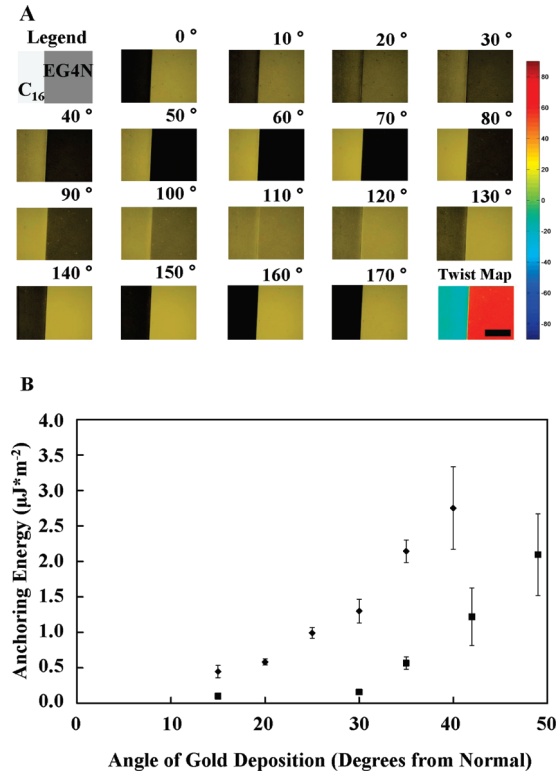

FIGURE 4. (A) Polarized light micrographs of a LC cell fabricated from obliquely deposited gold (35° angle of deposition) and functionalized with EG4N and hexadecanethiol (C16), as indicated in the legend. The LC optical cell was aligned such that the easy axis of the reference surface (see Materials and Methods) was parallel with the polarizer. The images were captured at various analyzer positions (as indicated; the angles denote the position of the analyzer relative to the crossed orientation of the polarizer and analyzer) and the twist angles of the LC were quantified as shown in the twist map (degrees of twist of the LC; see color scale). The scale bar represents 1 mm. (B) Azimuthal anchoring energy of nematic 5CB measured as a function of the angle of deposition of gold films for surfaces incubated with EG4N (squares) or EG4 (diamonds) at 1 mM concentration for 18 h. Error bars represent 95% confidence intervals for at least 3 samples.

favorably with a past study by Clare et al. (18). The results in Figure 4 also show that a gold deposition angle of 25° leads to an anchoring energy of 0.99 ± 0.08 μJ/m^2, which is within the optimal range of anchoring energies identified in the previous section of this paper. It is interesting to note that the uncertainty associated with the measured anchoring energies also increases with the gold deposition angle. As noted in the previous section, when measuring high anchoring energies, small uncertainties in the LC twist angle measurements lead to large uncertainties in the estimated value of anchoring energy (see Figure 3B).

Also shown in Figure 4 are the anchoring energies of SAMs formed from EG4N supported on obliquely deposited gold films. At angles of gold deposition of 15 and 30°, the anchoring energies measured on the two surfaces differed by only a small amount (0.10 ± 0.04 and 0.16 ± 0.03 μJ/m^2, respectively). However, for deposition angles between 30 and 49°, the anchoring energy again displayed a monotonic increase with the gold deposition angle, with the minimum value of 0.16 ± 0.03 μJ/m^2 occurring at 30° and a maximum value of 2.09 ± 0.58 μJ/m^2 occurring at 49°.

We conclude, therefore, that for SAMs formed from EG4N, the optimal anchoring energies for biomolecule detection are obtained with gold films deposited at angles between 35 and 42°. We also note that the uncertainty in anchoring energy increased with the deposition angle, and attempts to measure the anchoring energy of 5CB on SAMs formed from EG4N supported on gold films deposited at 64° led to uncertainties that obscured meaningful measurement of the anchoring energy.

The results above also clearly demonstrate that anchoring energies of 5CB on SAMs formed on obliquely deposited gold films do depend on the terminal functional group of the SAMs. A number of factors may underlie the difference in anchoring energy measured on SAMs formed from EG4 and EG4N. First, it may reflect differences in the intermolecular interactions of the mesogens with the amine and hydroxyl terminal groups of the SAMs. For example, the nitrile group of 5CB can hydrogen bond to the hydroxyl-terminated SAMs but not the amine-terminated SAMs. A second possible explanation for the difference in anchoring energies of nematic 5CB measured on the SAMs formed from EG4 and EG4N is the degree of ordering of the SAMs. Several past studies using Fourier transform infrared spectroscopy (FTIR) and chemical force titration measurements have shown that the degree of order within SAMs formed from 11-amino-1-undecanethiol can be lower/more variable than their methyl and hydroxyl-terminated analogues (55, 56). Consistent with these observations, for surfaces with similar magnitudes of anchoring energies, we measured the variability in anchoring energies to be greater for SAMs formed from EG4N than for SAMs formed from EG4 (1.22 ± 0.41 and 1.30 ± 0.17 μJ/m ^{2}, respectively). Finally, we note that Baio et al. (57) used X-ray photoelectron spectroscopy (XPS) to conclude that there exists substantial variation in the state of the amine group (free amine versus hydrochloride) of monolayers formed from 11-amino-1-undecanethiol depending upon the incubation time used to form the monolayers (57). Variation in the state of the terminal amine group of monolayers formed from EG4N may also contribute to the variability measured in the anchoring energies of LCs on these surfaces.

Effects of Thiol Incubation Time. Past studies have established that the degree of ordering of the molecules within SAMs formed from organothiols is dependent upon the structure of the organothiols as well as the conditions under which the SAMs are formed (e.g., temperature, time of incubation). Because the degree of ordering of a SAM likely influences the anchoring energy of a LC on the SAM (see discussion above), we predicted that the anchoring energy of a LC on a SAM may be influenced by the incubation time used to form the SAM. Such an effect, if observed, could potentially be used as an additional means by which to tune the anchoring energies of LCs on SAMs. Below we report on the influence of the incubation time (during formation of the SAM) on anchoring energies of LCs measured on SAMs formed from EG4N, EG3N, and EG4 on obliquely deposited gold films. We included SAMs formed from EG3N in our study to provide additional insight into the influence of amine-terminated SAMs on anchoring energies. We incubated the thiol solutions on obliquely deposited gold films for periods ranging from 2−192 h. These experimental conditions were guided by previous observations that various properties of ethylene glycol-terminated SAMs have been observed to evolve over a period of 3 days of incubation (58). We used gold films on which SAMs formed for 18 hours yielded anchoring energies of $\sim$2 μJ/m^2. This value of anchoring energy ($\sim$2 μJ/m^2) was selected because lower anchoring energies were expected to result from short incubation times (< 2 hours). For SAMs formed from either EG4N or EG3N, gold films deposited at 49° were used, whereas for SAMs formed from EG4, we used gold films deposited at an angle of 35°.

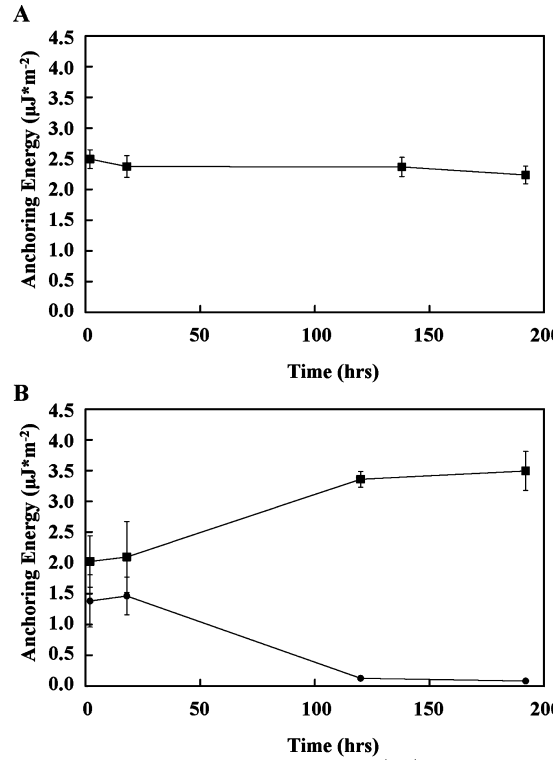

FIGURE 5. Azimuthal anchoring energy of nematic 5CB versus incubation time for SAMs formed from EG4, EG3N, EG4N. (A) EG4 thiol incubated against gold films deposited at 35° from the surface normal. (B) EG4N (squares) and EG3N (circles) thiols incubated (1 mM concentration) against gold films deposited at 49° from the surface normal. Error bars represent 95% confidence intervals for at least 3 samples.

The anchoring energies of nematic 5CB on SAMs formed from either EG4, EG4N or EG3N that were prepared using various incubation times are shown in Figure 5. Whereas the anchoring energies measured on the SAMs formed from EG4 were invariant (within experimental error) over $\sim$192 h of incubation (2.24 ± 0.14 μJ/m^2), Figure 5 shows that the amine-terminated SAMs (EG3N or EG4N) exhibited a complex behavior as a function of the time of incubation used to form the SAMs. Although at short times (less than 18 h), the anchoring energies measured on the two SAMs were similar, over longer incubation times (18−120 h) the anchoring energies measured on the two surfaces diverged in value. At very long times (greater than 120 h), the SAMs

formed from EG4N and EG3N reached time-invariant values. It is also interesting to note that the variability in the anchoring energy of the SAM formed from either EG4N or EG3N decreased after 18 hours of incubation (see relative sizes of the error bars in Figure 5B).

The constant value of the anchoring energy of the EG4 SAM (as a function of incubation time) suggests that the adsorption and ordering of the EG4 monolayer was rapid and largely complete within an hour. However, the anchoring energy of both amine-terminated SAMs (formed from EG3N or EG4N) changed significantly as a function of time when using incubation times between 18 and 120 h. We interpret this result to indicate that the kinetics of ordering of these SAMs is slow compared to SAMs formed from EG4. This interpretation is further supported by the observations that (i) the anchoring energies of SAMs formed from EG4N and EG3N were very similar for short incubation times ($\leq$ 18 h) and that (ii) they changed at nearly equal rates (but with opposite sign) over the range of incubation times we characterized. Finally, the observation that the anchoring energies of SAMs of EG4N and EG3N diverged over time indicates that the different number of EG units within EG3N and EG4N leads to substantially different interactions with 5CB. This result is consistent with past studies which have revealed that the number of repeat units within a SAM (methylene or ethyleneoxide) in contact with 5CB leads to different ordering of the 5CB (22, 35). We believe that the dependence of the orientation of the terminal amine group of the thiol monolayer on the number of the EG repeat units underlies the results shown in Figure 5B.

Mixed SAMs formed from EG4 and EG4N. Above we reported that SAMs prepared from EG4 and EG4N display different anchoring energies when formed on the same gold films (i.e., gold films deposited at the same angles of deposition). This result results suggests an additional approach by which to manipulate anchoring energies of LCs, namely, through control of the composition of mixed SAMs formed from EG4 and EG4N. We also comment that mixed monolayers prepared by co-adsorption of EG4 and EG4N are broadly useful for bioanalytical assays because the amine functionality of EG4N allows facile chemical functionalization, whereas the EG4 component minimizes adsorption of biomolecules. It is important to note that the surface composition of mixed SAMs does not necessarily match the bulk composition of the solution in contact with the surface, as the surface composition is determined by thermodynamic and kinetic factors (59). In particular, it has been reported that for co-adsorption of charged and neutral species, the surface adsorption of neutral species occurs preferentially compared to charged species (60).

We incubated solutions containing mixtures of EG4N and EG4 at a total thiol concentration of 1 mM on gold films that were deposited at an angle of 30°. We incubated all surfaces for the same length of time (18 hours). Figure 6 shows the anchoring energies of the mixed SAMs decreased from 1.30 $\pm$ 0.19 to 0.16 $\pm$ 0.06 μJ/m^2 as a linear function of the mole fraction of EG4N in the solution used to form the SAM. The

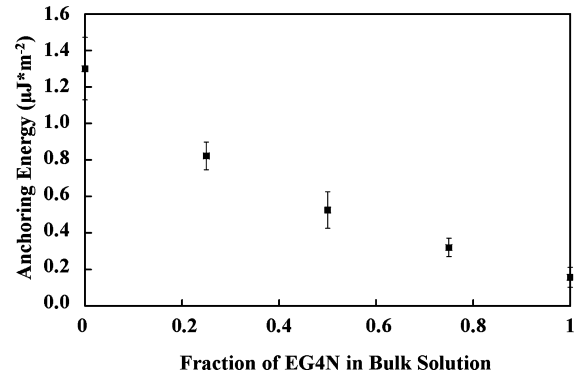

FIGURE 6. Azimuthal anchoring energy of nematic 5CB versus mole fraction of EG4N in an ethanolic solution containing EG4N and EG4 (1 mM total concentration) that was incubated against a gold film deposited at an angle of 30° from the surface normal. Error bars represent 95% confidence intervals for at least 3 samples.

SAMs that were rich in EG4 possessed anchoring energies that lie in the optimal range identified above. This simple result, when combined with the results described in the previous section, indicate that manipulation of the composition of a mixed SAM along with the angle of deposition of the supporting gold film can be used to design surfaces with a desired density of terminal amine groups while maintaining an optimal value of the anchoring energy for LC-based detection of biomolecules.

Affinity Contact Printing of EGFR. Using the surfaces identified above, we next sought to determine if the response of the LC (change in twist angle) to surface-bound proteins would depend on the anchoring energy of the surfaces on which the proteins were presented or the thickness of the LC film (as predicted in Figure 3). Here, we note that past studies have shown that proteins bound to SAMs formed on obliquely deposited gold films cause a decrease in the anchoring energy of nematic phases of 5CB on those surfaces (17). To characterize the response of the LC to protein bound to surfaces that possessed different anchoring energies (prior to deposition of the protein), we utilized affinity contact printing to transfer EGFR onto SAMs prepared from EG4N (41). The affinity contact printing utilized an anti-EGFR antibody covalently linked to the surface of a PDMS stamp. Following incubation in a solution of EGFR, the surface of the stamp was rinsed, dried and placed into conformal contact with a solid surface, thus transferring the affinity captured EGFR to the solid surface. Because EGFR undergoes autophosphorylation in the presence of EGF (61), it was possible to radioactivity label EGFR using [γ-^{32}P] ATP and thereby independently quantify the capture and transfer of the EGFR to the analytic surface (41). We chose to transfer the EGFR to the SAMs formed from EG4N because the amine-functional group of EG4N promotes the capture of EGFR from the antibody-functionalized PDMS stamp (41, 62). By using scintillation counting of the radio-labeled EGFR, we determined that the transfer of EGFR from the affinity capture stamp to the EG4N-decorated surfaces in the experiments reported below ranged from 30

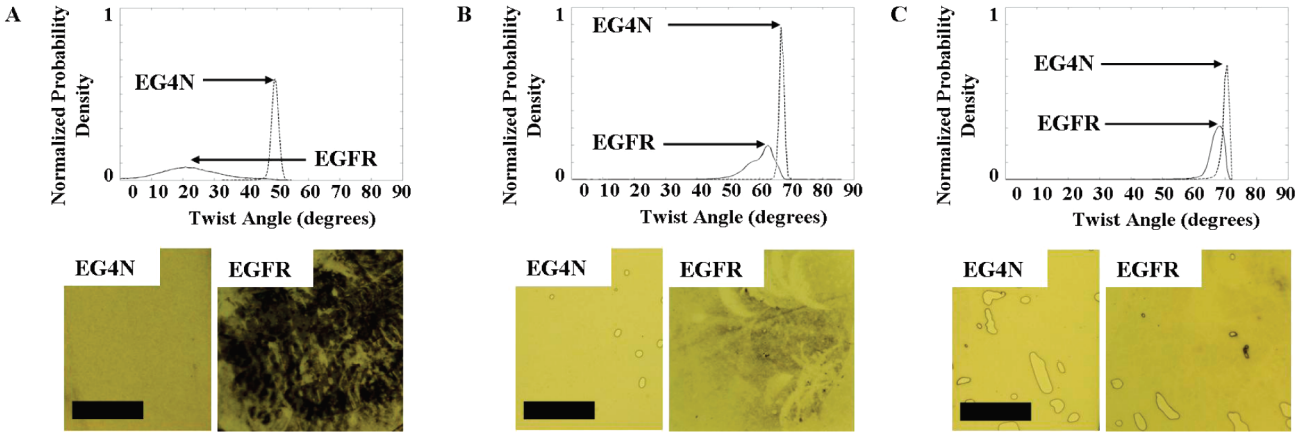

FIGURE 7. Normalized distributions of twist angles (top) and the corresponding polarized light micrographs (bottom) of nematic LCs on surfaces that were prepared by obliquely depositing gold films at (A) 35 and (B, C) 49°, and subsequently functionalized with EG4N (dotted lines) and decorated with EGFR using affinity contact printing (solid lines). Samples A and B had LC film thicknesses of 16 μm. The LC optical cells were aligned between crossed polarizers such that the easy axes of the reference surfaces (see Materials and Methods) were parallel to the polarizer. The scale bars represent 1 mm.

to 40 pg/mm ^{2}. For the surface areas used in our study (10 mm^2), the total mass of captured EGFR was 0.3−0.4 ng (2−3 fmol).

We fabricated TNLC cells to investigate the response of LC to the surface-bound EGFR in three regions of the plot shown in Figure 3B (hereafter referred to as Schemes 1−3). For Schemes 1 and 2, we maintained the thickness of the LC constant at 16 μm, and investigated the consequence of an increase in anchoring energy of the LC on the analytic surface (from 0.6 μJ/m^2 in Scheme 1 to 2.1 μJ/m^2 in Scheme 2) on the response of the LC to the presence of EGFR. The anchoring energy of the surfaces used in Schemes 1 and 2 were engineered by changing the angle of deposition of the gold films (35° for Scheme 1 and 49° for Scheme 2) used to support the SAM formed from EG4N. Scheme 3 used surfaces fabricated from gold films that were obliquely deposited at an angle of 49° (same as Scheme 2) in combination with a LC film with a thickness of 50 μm. When combined, the experiments performed using Scheme 2 and 3 were designed to enable evaluation of the impact of the LC film thickness (16 μm versus 50 μm, at constant anchoring energy) on the response of the LC to surface-bound EGFR.

Results obtained using Schemes 1−3 are shown in Figure 7, where the distributions of twist angles within the films of LC on the analytic surfaces are presented (measured for each 5 μm × 5 μm pixel on the surface) along with polarized optical micrographs of the LC cells. For each scheme, we measured the distribution of twist angles on the region of the analytic surface that was decorated with the EGFR as well as a region of the surface that was free of EGFR. All measurements were performed with at least three replicates.

Figure 7A shows the results obtained using the analytic surface with an anchoring energy of 0.6 μJ/m^2 and an LC film thickness of 16 μm (Scheme 1). Inspection of Figure 7A reveals that the distribution of twist angles of the LC was narrow (FWHM = 2.8°) and centered around 49.3° on regions of the SAM formed from EG4N that were free of EGFR. This narrow distribution of twist angles is reflected in the homogenous appearance of the associated polarized optical micrograph shown at the bottom of Figure 7A. In contrast, the distribution of twist angles on the regions of the SAM presenting the EGFR differed from the EGFR-free regions by (i) the average value of the twist angle (~21.9°) and (ii) the width of the distribution of twist angles (FWHM = 22.8°). The change in the average values of the twist angle of the LC (49.3−21.9°) that were induced by the presence of the EGFR corresponds to a reduction in anchoring energy of 0.4 μJ/m^2. We also note that the substantial increase in the width of the distribution of twist angles of the LC on the EGFR-decorated regions of the surface indicates that the affinity contact printing of the EGFR on the surface leads to a structurally heterogenous surface, likely due to differences in the local density and/or state of the EGFR deposited onto the SAM. This heterogeneity is evident in the associated polarized optical micrograph shown at the bottom of Figure 7A.

A comparison of the results presented in panels A and B in Figure 7 permits assessment of the influence of the anchoring energy of the analytic surface on the response of the LC to the surface-bound EGFR (at a constant LC film thickness of 16 μm). As mentioned above, the surfaces used to obtain the data in Figure 7A possessed anchoring energies of 0.6 μJ/m^2 whereas the surfaces used to obtain Figure 7B possessed an anchoring energy of 2.1 μJ/m^2. We make three observations based on the comparison of panels A and B in Figure 7. First, the twist angle of the LC measured on the SAMs formed from EG4N that were free of EGFR is greater in Figure 7B (66.9°) than Figure 7A (49.3°); this relative ranking reflects the differences in the anchoring energies of the two surfaces. Second, the change in the average twist angle (66.9−59.8°) caused by the surface-bound EGFR is smaller in Figure 7B as compared to Figure 7A. Although the change in twist angle is smaller, when expressed in terms of a change in anchoring energy, the change in anchoring energy induced by EGFR is greater in Figure 7B (2.1−1.1 μJ/m^2) than Figure 7A (0.6−0.2 μJ/m^2). This result is an interesting one, as it suggests that the change in anchoring energy

induced by a given density of protein on a surface is dependent on the anchoring energy of the surface prior to deposition of the protein. Finally, we also note that the width of the distribution of twist angles measured after the affinity contact printing of the EGFR is smaller in Figure 7B as compared to 7A. This relatively narrower distribution of twist angles can be observed qualitatively in the associated polarized micrograph shown at the bottom right of Figure 7B, which shows a less obvious change in light transmission as compared to the image in the bottom right of Figure 7A. We note that the small circular defects in the polarized micrographs in the bottom right image of Figure 7B are the result of domains of the LC that were twisted in the opposite sense (i.e., counter-clockwise rather than clockwise). These domains are more likely to occur in twisted LCs systems that do not have high values of φ (refer to Figure 2A) (63).

Figure 7C shows the distribution of twist angles obtained using the same surfaces as used in Figure 7B (anchoring energies of 2.1 μJ/m^2), but with thicker LC films (50 μm thickness, whereas the data in Figure 7B were obtained using LC films with thickness of 16 μm). The effect of the thickness of the LC film on the distribution of twist angles of the LC is two-fold. First, because the thick LC film decreases the torque that the twisted LC exerts on the analytic surface (for a given twist angle), we observed the twist angles measured in Figure 7C in the absence of surface-bound EGFR (69.5°) to be larger than those measured in Figure 7B (66.9°). Second, we observe the response of the LC (change of twist angle) induced by the surface-bound EGFR to be small in Figure 7C (69.5−66.4°), as compared to Figure 7B (66.9−59.8°). Here again, this relative ranking of the response of the LC to the EGFR reflects the magnitude of the torque applied by the LC at the analytic surface. For thick LC films, the torque applied by the LC is small and thus the LC departs by only a small angle from the orientation of the easy axis of the analytic surface. This leads to the relatively homogenous appearance of the associated polarized optical micrographs (bottom right of Figure 7C), where the only obvious features are the small domains of LC with opposite handedness of twist (see above). It is interesting to note, however, that the EGFR-induced change in anchoring energy calculated from the results shown in Figure 7C is 1.2 μJ/m^2, a value that is similar to that calculated from Figure 7B. This result provides further support for our conclusion that the change in anchoring energy of a surface induced by bound protein is a function of the anchoring energy of the surface. Finally, we note that control experiments (using isotype control antibodies on the PDMS surface) were performed for Schemes 1−3 to confirm that the response of the LC was a result of specifically bound EGFR (see the Supporting Information).

The results reported above, when combined, indicate that the largest change in twist angle induced by the presence of the EGFR is encountered when using surfaces with the lowest anchoring energy and thinnest LC films. This relative ranking of the response (when expressed in terms of the change in twist angle of the LC) is also consistent with the visual appearance of the LC cells, when viewed between crossed polarizers. When using the surface with the low anchoring energy and thin LC film (Scheme 1), the area of the surface decorated with EGFR was easily distinguished (by visual inspection) from the EG4N region of the surface that was free from EGFR. For the surfaces used in Scheme 2, the response of the LC on the area of the surface presenting the EGFR was only faintly visible when viewed between crossed polarizers. Finally, it was not possible to visualize the presence of the EGFR on the surfaces used to obtained data for Scheme 3.

In summary, the results presented above lead us to three main conclusions: (i) 30−40 pg/mm^2 of EGFR bound to a SAM formed from EG4N was easily detected using the twisted LC cells, (ii) the presence of EGFR on the surface caused the LC twist angle to decrease, and exhibit a broad distribution of twist angles, with the decrease in average twist angle and increase in width of distribution being greatest on the surfaces with the lowest anchoring energy surface, and (iii) the use of thin LC cells lead to maximal changes in LC twist angle induced by the presence of the EGFR on the surface. Finally, we note that we have previously demonstrated that it is possible to spatially resolve LC twist angles on regions of surfaces with a resolution of ~10 μm. Thus, in principle, it should be feasible to detect the presence of EGFR captured on small regions of surfaces. We calculate that the amount of EGFR on a 10 μm × 10 μm area of a surface with a surface density of 30 pg/mm^2 to be 0.3 fg. This quantity of EGFR is comparable to the mass of EGFR associated with individual mammalian cells of many different cell lines (50 000−500 000 molecules/cell or 0.02−0.2 pg/cell) (64). We note that lysis of a single cell within a microwell (65) of size 20 μm × 20 μm × 20 μm dimensions would lead to a concentration of EGFR of ~30 nM, a concentration that is comparable to that used in this study (~2 nM). In future studies, we will report on detection of EGFR from small numbers of cells.

CONCLUSIONS

The key conclusions of the study reported in this paper are threefold. First, a simple analysis of the torque-balance equation has led us to identify a range of surface anchoring energies and LC film thicknesses that we predicted would provide a maximal response of a twisted LC to protein captured on a surface. The optimal anchoring energies lie in the range of 0.5 to 2.0 μJ/m^2 when using nematic 5CB. Second, we have demonstrated several methods that permit manipulation of the anchoring energies of surfaces so as to obtain values identified as being optimal. These surfaces possessed chemical functionality that enabled the capture of proteins on the surfaces via affinity contact printing. Finally, by using the EGFR in combination with affinity contact printing, we demonstrated that the essential predictions of the torque-balance model are correct. Our results confirm that the LC response to the presence of 30−40 pg/mm^2 of EGFR was higher when low anchoring energy surfaces (~0.6 μJ/m^2) and thin LC films (16 μm thickness) were used. Overall, the results presented in this paper

advance the design of surfaces for use in bioanalytical methods that employ surface-driven ordering transitions in LCs.

Acknowledgment. The authors acknowledge Gary M. Koenig for helpful discussions. This research was partially supported by the National Science Foundation (DMR 0079983) and the National Institutes of Health (CA108467 and CA105730).

Supporting Information Available: Details related to the preparation, capture, and quantification of affinity contact printed EGFR; polarized light micrographs that were used to calculate the anchoring energy of 5CB in contact with SAMs formed from EG4 and EG3N (PDF). This material is available free of charge via the Internet at http://pubs.acs.org.

REFERENCES AND NOTES

(1) Southern, E. M.; Maskos, U.; Elder, J. K. *Genomics* **1992**, *13*, 1008–1017.
(2) Gorg, A.; Weiss, W.; Dunn, M. J. *Proteomics* **2004**, *4*, 3665–3685.
(3) Emili, A. Q.; Cagney, G. *Nat. Biotechnol.* **2000**, *18*, 393–397.
(4) Fodor, S. P. A.; Read, J. L.; Pirrung, M. C.; Stryer, L.; Lu, A. T.; Solas, D. *Science* **1991**, *251*, 767–773.
(5) Kingsmore, S. F. *Nat. Rev. Drug Discovery* **2006**, *5*, 310–320.
(6) Schweitzer, B.; Roberts, S.; Grimwade, B.; Shao, W. P.; Wang, M. J.; Fu, Q.; Shu, Q. P.; Laroche, I.; Zhou, Z. M.; Tchernev, V. T.; Christiansen, J.; Velleca, M.; Kingsmore, S. F. *Nat. Biotechnol.* **2002**, *20*, 359–365.
(7) de Wildt, R. M. T.; Mundy, C. R.; Gorick, B. D.; Tomlinson, I. M. *Nat. Biotechnol.* **2000**, *18*, 989–994.
(8) Duggan, D. J.; Bittner, M.; Chen, Y. D.; Meltzer, P.; Trent, J. M. *Nat. Genet.* **1999**, *21*, 10–14.
(9) Stelzl, U.; Worm, U.; Lalowski, M.; Haenig, C.; Brembeck, F. H.; Goehler, H.; Stroedicke, M.; Zenkner, M.; Schoenherr, A.; Koeppen, S.; Timm, J.; Mintzlaff, S.; Abraham, C.; Bock, N.; Kietzmann, S.; Goedde, A.; Toksoz, E.; Droege, A.; Krobitsch, S.; Korn, B.; Birchmeier, W.; Lehrach, H.; Wanker, E. E. *Cell* **2005**, *122*, 957–968.
(10) Rual, J. F.; Venkatesan, K.; Hao, T.; Hirozane-Kishikawa, T.; Dricot, A.; Li, N.; Berriz, G. F.; Gibbons, F. D.; Dreze, M.; Ayivi-Guedehoussou, N.; Klitgord, N.; Simon, C.; Boxem, M.; Milstein, S.; Rosenberg, J.; Goldberg, D. S.; Zhang, L. V.; Wong, S. L.; Franklin, G.; Li, S. M.; Albala, J. S.; Lim, J. H.; Fraughton, C.; Llamosas, E.; Cevik, S.; Bex, C.; Lamesch, P.; Sikorski, R. S.; Vandenhaute, J.; Zoghbi, H. Y.; Smolyar, A.; Bosak, S.; Sequerra, R.; Doucette-Stamm, L.; Cusick, M. E.; Hill, D. E.; Roth, F. P.; Vidal, M. *Nature* **2005**, *437*, 1173–1178.
(11) MacBeath, G. *Nat. Genet.* **2002**, *32*, 526–532.
(12) Voller, A.; Bartlett, A.; Bidwell, D. E. *J. Clin. Pathol.* **1978**, *31*, 507–520.
(13) Nielsen, U. B.; Geierstanger, B. H. *J. Immunol. Methods* **2004**, *290*, 107–120.
(14) Homola, J. *Chem. Rev.* **2008**, *108*, 462–493.
(15) Yang, S. Y.; Xiao, X. Y.; Zhang, W. G.; Zhang, L. J.; Zhang, W.; Zhou, B.; Chen, G.; He, D. C. *BMC Cancer* **2005**, *5*, 7.
(16) Lee, K. B.; Park, S. J.; Mirkin, C. A.; Smith, J. C.; Mrksich, M. *Science* **2002**, *295*, 1702–1705.
(17) Govindaraju, T.; Bertics, P. J.; Raines, R. T.; Abbott, N. L. *J. Am. Chem. Soc.* **2007**, *129*, 11223–11231.
(18) Clare, B. H.; Guzman, O.; de Pablo, J. J.; Abbott, N. L. *Langmuir* **2006**, *22*, 7776–7782.
(19) Lowe, A. M.; Bertics, P. J.; Abbott, N. L. *Anal. Chem.* **2008**, *80*, 2637–2645.
(20) Faetti, S.; Marianelli, P. *Phys. Rev. E: Stat., Nonlinear, Soft Matter Phys.* **2005**, *72*, 9.
(21) Clare, B. H.; Abbott, N. L. *Langmuir* **2005**, *21*, 6451–6461.
(22) Clare, B. H.; Guzman, O.; de Pablo, J. J.; Abbott, N. L. *Langmuir* **2006**, *22*, 4654–4659.
(23) Bryan-Brown, G. P.; Wood, E. L.; Sage, I. C. *Nature* **1999**, *399*, 338–340.
(24) Yeung, F. S. Y.; Ho, Y. L. J.; Li, Y. W.; Kwok, H. S. *J. Disp. Technol.* **2008**, *4*, 24–27.
(25) Thieghi, L. T.; Barberi, R.; Bonvent, J. J.; Oliveira, E. A.; Giacometti, J. A.; Balogh, D. T. *Phys. Rev. E: Stat., Nonlinear, Soft Matter Phys.* **2003**, *67*, 6.
(26) Nespoulous, M.; Blanc, C.; Nobili, M. *J. Appl. Phys.* **2007**, *102*, 7.
(27) Vondeimling, A.; Louis, D. N.; Wiestler, O. D. *Glia* **1995**, *15*, 328–338.
(28) Cowley, G. P.; Smith, J. A.; Gusterson, B. A. *Br. J. Cancer* **1986**, *53*, 223–229.
(29) Fonseca, J. G.; Galerne, Y. *Appl. Phys. Lett.* **2001**, *79*, 2910–2912.
(30) Stohr, J.; Samant, M. G.; Luning, J.; Callegari, A. C.; Chaudhari, P.; Doyle, J. P.; Lacey, J. A.; Lien, S. A.; Purushothaman, S.; Speidell, J. L. *Science* **2001**, *292*, 2299–2302.
(31) Schadt, M.; Seiberle, H.; Schuster, A. *Nature* **1996**, *381*, 212–215.
(32) Skaife, J. J.; Brake, J. M.; Abbott, N. L. *Langmuir* **2001**, *17*, 5448–5457.
(33) Goodman, L. A.; McGinn, J. T.; Anderson, C. H.; Digeronimo, F. *IEEE Trans. Electron Devices* **1977**, *ED24*, 795–804.
(34) Russell, J. M.; Oh, S. J.; LaRue, I.; Zhou, O.; Samulski, E. T. *Thin Solid Films* **2006**, *509*, 53–57.
(35) Gupta, V. K.; Abbott, N. L. *Phys. Rev. E: Stat., Nonlinear, Soft Matter Phys.* **1996**, *54*, R4540–R4543.
(36) Luk, Y. Y.; Tingey, M. L.; Hall, D. J.; Israel, B. A.; Murphy, C. J.; Bertics, P. J.; Abbott, N. L. *Langmuir* **2003**, *19*, 1671–1680.
(37) Willey, T. M.; Vance, A. L.; van Buuren, T.; Bostedt, C.; Terminello, L. J.; Fadley, C. S. *Surf. Sci.* **2005**, *576*, 188–196.
(38) Lee, M. T.; Hsueh, C. C.; Freund, M. S.; Ferguson, G. S. *Langmuir* **1998**, *14*, 6419–6423.
(39) Cortes, E.; Rubert, A. A.; Benitez, G.; Carro, P.; Vela, M. E.; Salvarezza, R. C. *Langmuir* **2009**, *25*, 5661–5666.
(40) Wiepz, G. J.; Guadaramma, A. G.; Fulgham, D. L.; Bertics, P. J. In *Epidermal Growth Factor Methods and Protocols*; PatelT. B., Ed.; Methods in Molecular Biology; Humana Press: Totowa, NJ, 2006; Vol. 327, pp 2538.
(41) Lowe, A. M.; Ozer, B. H.; Wiepz, G. J.; Bertics, P. J.; Abbott, N. L. *Lab Chip* **2008**, *8*, 1357–1364.
(42) Lien, A. In *Conference Record of the 1991 International Display Research Conference*; San Diego, Oct 15—17, 1991; IEEE: Piscataway, NJ, 1991; pp 192—194.
(43) Toyooka, T.; Chen, G.; Takezoe, H.; Fukuda, A. *Jpn. J. Appl. Phys.* **1987**, *26*, 1959–1966.
(44) Everitt, D. L.; Miller, W. J. W.; Abbott, N. L.; Zhu, X. D. *Phys. Rev. B: Condens. Matter Mater. Phys.* **2000**, *62*, R4833–R4836.
(45) Berreman, D. W. *Mol. Cryst. Liq. Cryst.* **1973**, *23*, 215–231.
(46) Kane, R. S.; Deschatelets, P.; Whitesides, G. M. *Langmuir* **2003**, *19*, 2388–2391.
(47) Li, L. Y.; Chen, S. F.; Jiang, S. Y. *J. Biomater. Sci., Polym. Ed.* **2007**, *18*, 1415–1427.
(48) Harder, P.; Grunze, M.; Dahint, R.; Whitesides, G. M.; Laibinis, P. E. *J. Phys. Chem. B* **1998**, *102*, 426–436.
(49) Herrwerth, S.; Eck, W.; Reinhardt, S.; Grunze, M. *J. Am. Chem. Soc.* **2003**, *125*, 9359–9366.
(50) Jang, C. H.; Tingey, M. L.; Korpi, N. L.; Wiepz, G. J.; Schiller, J. H.; Bertics, P. J.; Abbott, N. L. *J. Am. Chem. Soc.* **2005**, *127*, 8912–8913.
(51) Tingey, M. L.; Snodgrass, E. J.; Abbott, N. L. *Adv. Mater.* **2004**, *16*, 1331–1336.
(52) Tingey, M. L.; Wilyana, S.; Snodgrass, E. J.; Abbott, N. L. *Langmuir* **2004**, *20*, 6818–6826.
(53) Faucheux, N.; Schweiss, R.; Lutzow, K.; Werner, C.; Groth, T. *Biomaterials* **2004**, *25*, 2721–2730.
(54) Lee, M. H.; Brass, D. A.; Morris, R.; Composto, R. J.; Ducheyne, P. *Biomaterials* **2005**, *26*, 1721–1730.
(55) Wang, H.; Chen, S. F.; Li, L. Y.; Jiang, S. Y. *Langmuir* **2005**, *21*, 2633–2636.
(56) Wallwork, M. L.; Smith, D. A.; Zhang, J.; Kirkham, J.; Robinson, C. *Langmuir* **2001**, *17*, 1126–1131.
(57) Baio, J. E.; Weidner, T.; Brison, J.; Graham, D. J.; Gamble, L. J.; Castner, D. G. *J. Electron Spectrosc. Relat. Phenom.* **2009**, *172*, 2–8.
(58) Vanderah, D. J.; Arsenault, J.; La, H.; Gates, R. S.; Silin, V.; Meuse, C. W.; Valincius, G. *Langmuir* **2003**, *19*, 3752–3756.
(59) Bain, C. D.; Evall, J.; Whitesides, G. M. *J. Am. Chem. Soc.* **1989**, *111*, 7155–7164.
(60) Doneux, T.; De Decker, Y. *Langmuir* **2009**, *25*, 2199–2203.
(61) Ullrich, A.; Schlessinger, J. *Cell* **1990**, *61*, 203–212.
(62) Tan, J. L.; Tien, J.; Chen, C. S. *Langmuir* **2002**, *18*, 519–523.
(63) Miyaji, A.; Yamaguchi, M.; Toda, A.; Mada, H.; Kobayashi, S. *IEEE Trans. Electron Devices* **1977**, *24*, 811–815.
(64) Boonstra, J.; Delaat, S. W.; Ponec, M. *Exp. Cell Res.* **1985**, *161*, 421–433.
(65) Sasuga, Y.; Iwasawa, T.; Terada, K.; Oe, Y.; Sorimachi, H.; Ohara, O.; Harada, Y. *Anal. Chem.* **2008**, *80*, 9141–9149.

AM900753V